Supporting information for

Solar driven renewable energy storage using rhenium disulfide nanostructure based rechargeable supercapacitors

Parthiban Pazhamalai,[a] Karthikeyan Krishnamoorthy,[a] Vimal Kumar Mariappan,[a]

Arunprasath Sathyaseelan,[a] Sang -Jae Kim,[a, b, *]

[a] Nanomaterials & System Laboratory, Major of Mechatronics Engineering,

Faculty of Applied Energy System, Jeju National University, Jeju 63243, Republic of Korea

[b]Department of Advanced Convergence Science and Technology, Jeju National University,

Jeju 63243, Republic of Korea

*Corresponding author Email: kimsangj@jejunu.ac.kr

S1. Experimental section

S1.1 Materials

Ammonium perrhenate (NH_4ReO_4) was obtained from Alfa-aesar private Ltd., South Korea. Hydroxylamine hydrochloride ($HONH_3Cl$), lithium sulfate, and thiourea (CH_4N_2S) were purchased from Daejung Chemicals Ltd., South Korea.

S1.2 Preparation of rhenium disulfide (ReS_2) nanostructures

A facile hydrothermal method was employed for the preparation of ReS_2 nanostructures according to the methods available in literature[1,2]. At first, ammonium perrhenate (0.161 g), hydroxylamine hydrochloride (0.125 g), and thiourea (0.205 g) were dissolved in 50 mL of DI water and stirred for 30 min. Then, the mixture solution was transferred to an 80 mL stainless steel autoclave for hydrothermal reaction at a temperature of 240 ℃ and kept for 24 h. After completion of the reaction, the reactor was allowed to cool down to room temperature naturally. Then, the black colored precipitates containing ReS_2 was repeatedly washed with DI water and ethanol using centrifugation process and dried at 80 ℃ for 12 h.

S1.3 Instrumentation

The phase purity and the crystallinity of the ReS_2 nanostructures were determined using Rigaku X-ray diffractometer operated at 40 keV and 40 mA Cu Kα radiation. The Raman spectra of the ReS_2 nanostructures were obtained using Lab Ram HR Evolution Raman spectrometer (Horiba Jobin-Yvon, France). The Raman system was operated at 10 mW laser power and an excitation wavelength of 514 nm with an Ar^+ ion laser. The data were collected using a 10 s data point acquisition time. The chemical composition and state of elements present in ReS_2 were obtained by X-ray photoelectron spectroscopy (XPS) techniques using ESCA-2000, VG Microtech Ltd. In this, a monochromatic X-ray beam source at 1486.6 eV (aluminum anode) and

14 kV was used to scan the sample surface. A high-flux X-ray source with an aluminum anode was used for X-ray generation, and a quartz crystal monochromator was used to focus and scan the X-ray beam on the sample. The elemental mapping and morphology of the ReS_2 nanostructures was examined using field-emission scanning electron microscope (TESCAN – MIRA3) instrument. The surface morphology of the ReS_2 nanostructures was analyzed using transmission emission scanning electron microscope (HR-TEM, JEOL JEM 2011, JEOL Ltd.).

S1.4 Electrochemical studies

The ReS_2 electrode for the electrochemical studies were according to the slurry coating procedure reported in our previous work[3]. Briefly, the active material (ReS_2), carbon black and polyvinylidene difluoride (PVDF) were mixed the ratio of 85:10:5 using N-methyl pyrrolidone (NMP) as solvent and ground well to form the slurry. Then, the prepared slurry was coated on to the pre-cleaned SS substrate (1×1 cm^2) and allowed to dry at 80 ºC overnight. The electroactive mass of the ReS_2 electrode on to the stainless-steel substrate is calculated from the difference between the mass of the substrate before and after coating of the ReS_2 electrode using Dual-range Semi-micro Balance (AUW-220D, SHIMADZU) with an approximation of five-decimal points is approximate ~ 0.7 mg in each substrate. The electrochemical characterization of the ReS_2 electrode was examined using a three-electrode system. Here, the ReS_2 electrode was used as the working electrode, silver/silver chloride as the reference electrode, and platinum as the counter electrode. The ReS_2 symmetric capacitors (two-electrode) were fabricated in the form of a sandwich-type electrode, with an electrolyte-immersed Celgard as the separator. The electrochemical properties were examined via cyclic voltammetry (CV), electrochemical impedance spectroscopy (EIS) and galvanostatic charge-discharge (CD) measurements using an

Autolab PGSTAT302N electrochemical workstation. An aqueous solution containing 1 M Li_2SO_4 was used as an electrolyte.

S1.5 Electrochemical analysis

S1.5.1 Determination of specific capacitance from CV profiles:

The specific capacitance of the ReS_2 SSC device was calculated from the CV analysis using the relation[4]:

$$C = [\int IdV / (s \times \Delta V \times M)] \quad (1)$$

Here "C" is the specific capacitance (F g^{-1}) of SSC device, "I" is the current (A), "s" is the scan rate (mV s^{-1}), "ΔV" is the potential window (V), and "M" is the mass of the electrode (g).

S1.5.2 Determination of specific capacitance, Columbic efficiency, energy and power density values from CD profiles:

The specific capacitance, Columbic efficiency (η%), energy and power density of the ReS_2 SSC device was obtained from the CD analysis using the relations[5,6]:

$$C_s = (I \times t_d) / (M \times \Delta V) \quad (2)$$

$$E = (Cs \times \Delta V^2)/2 \quad (3)$$

$$P = E/t_d \quad (4)$$

Here "C_s" is the specific capacitance, "E" is the energy density, "P" is the power density, "I" is the discharge current density, "t_c" is the charging time, "t_d" is the discharge time, "M" is the mass of the electroactive material and "ΔV" is the potential window.

S1.5.3 Determination of real and imaginary components of capacitance from EIS analysis:

The variation of real and imaginary capacitance of ReS_2 SSC device with respect to the applied range of frequencies was obtained using the relation (6) and (7) respectively[3]:

$$C'_{\omega} = -Z''_{\omega} /(\omega|Z_{\omega}|^2) \ldots\ldots\ldots\ldots (6)$$

$$C''_{\omega} = Z'_{\omega} /(\omega|Z_{\omega}|^2) \ldots\ldots\ldots\ldots (7)$$

Here, "C'_{ω}" and "C''_{ω}" represents the real and imaginary components of capacitance that corresponds to the stored energy and irreversible energy loses, respectively.

S1.5.4 Determination of specific capacitance from EIS analysis:

The variation of ReS_2 SSC device capacitance with respect to the applied frequency with an increase in potential using the relation[7]:

$$C_s = -1/2\pi f z'' \ldots\ldots\ldots\ldots (8)$$

Here *"C_s"* is the specific capacitance of the device, and *"f"* is the applied frequency, and *"z''"* is the imaginary plot of impedance.

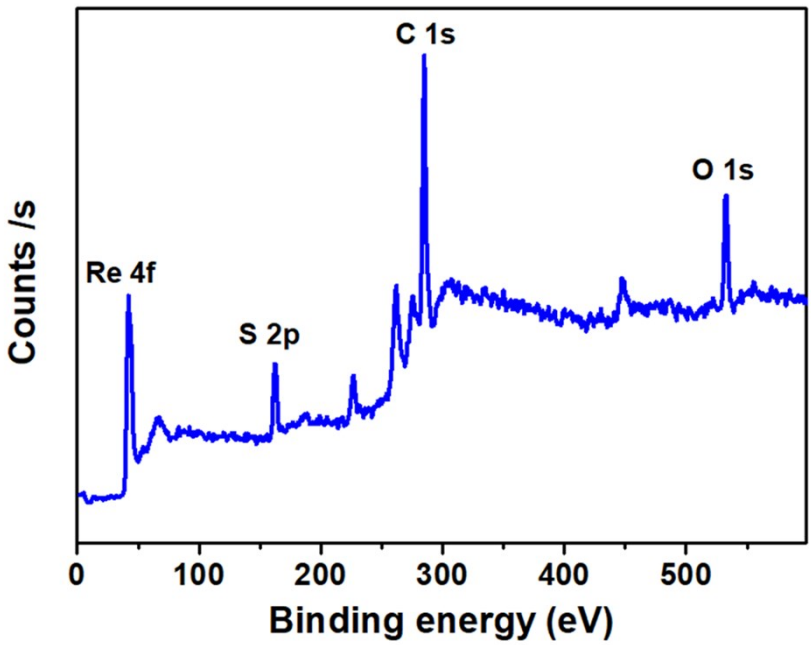

Figure S1. Typical X-ray photoelectron survey spectrum of the hydrothermally prepared ReS_2 nanostructures showing the presence of Re, S components in addition to C and O components.

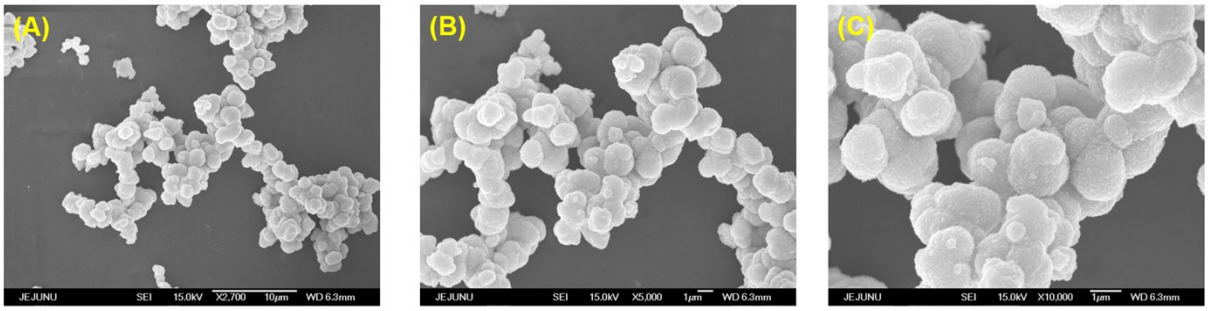

Figure S2 FESEM micrograph of ReS_2 nanostructures (A) low magnification and (B and C) high magnification.

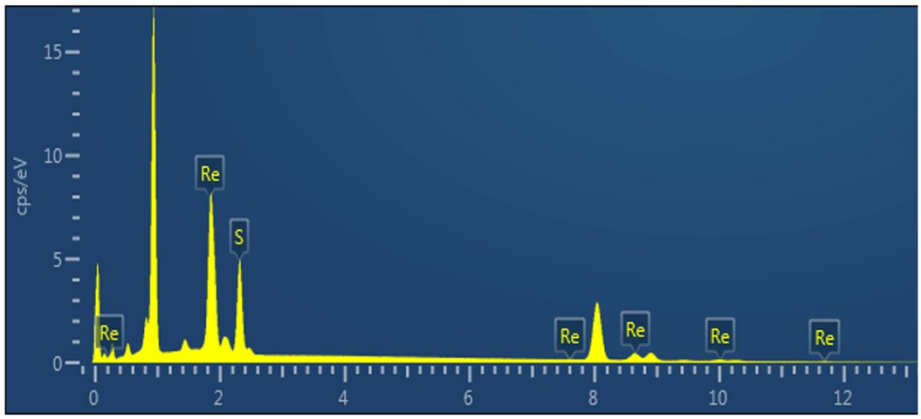

Figure S3. Energy disperspersive X-ray spectrum of hydrothermally prepared ReS_2.

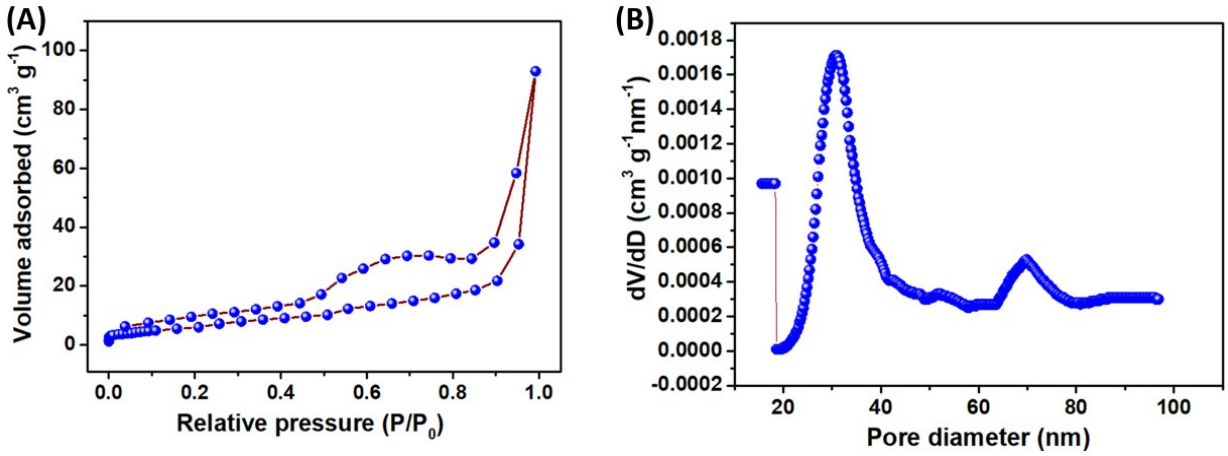

Figure S4. Surface area analysis of ReS_2 nanostructures (A) N_2 adsorption/desorption isotherm (B) Pore volume distribution.

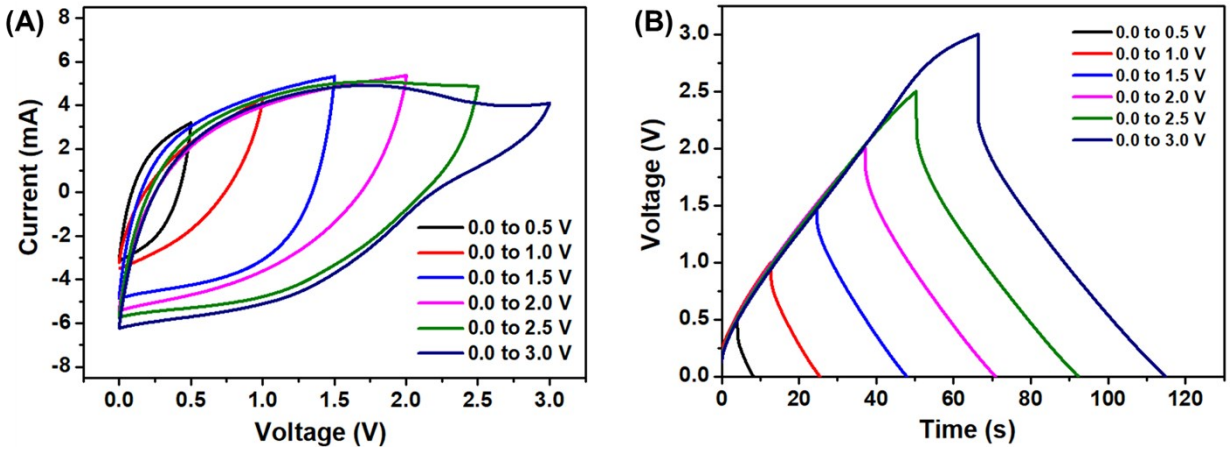

Figure S5. Electrochemical characterization of ReS_2 SSC device using 1M $TEABF_4$ as electrolyte. (A) CV and (B) CD profiles measured at various OPWs.

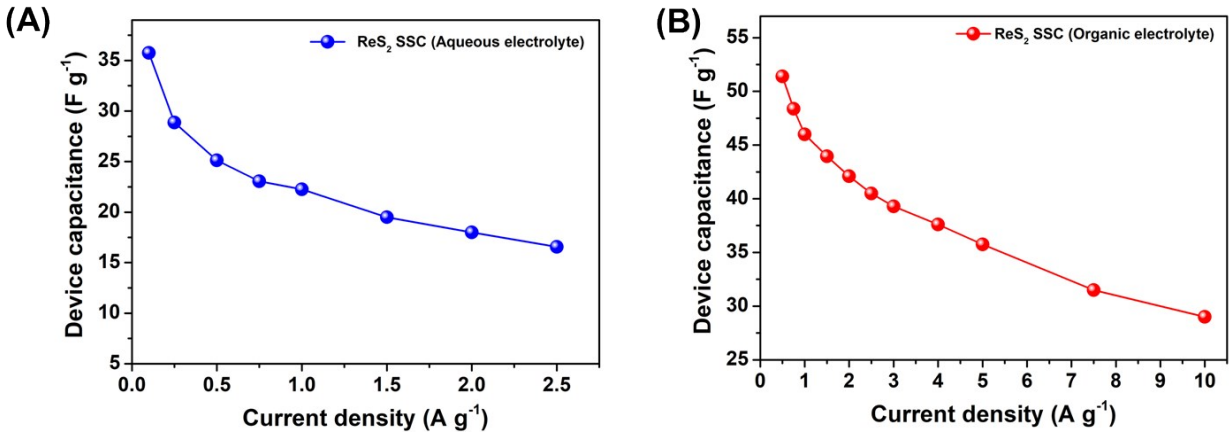

Figure S6. Effect of current density on the specific capacitance of the ReS_2 SSC device (A) 1 M Li_2SO_4 and (B) 1 M $TEABF_4$

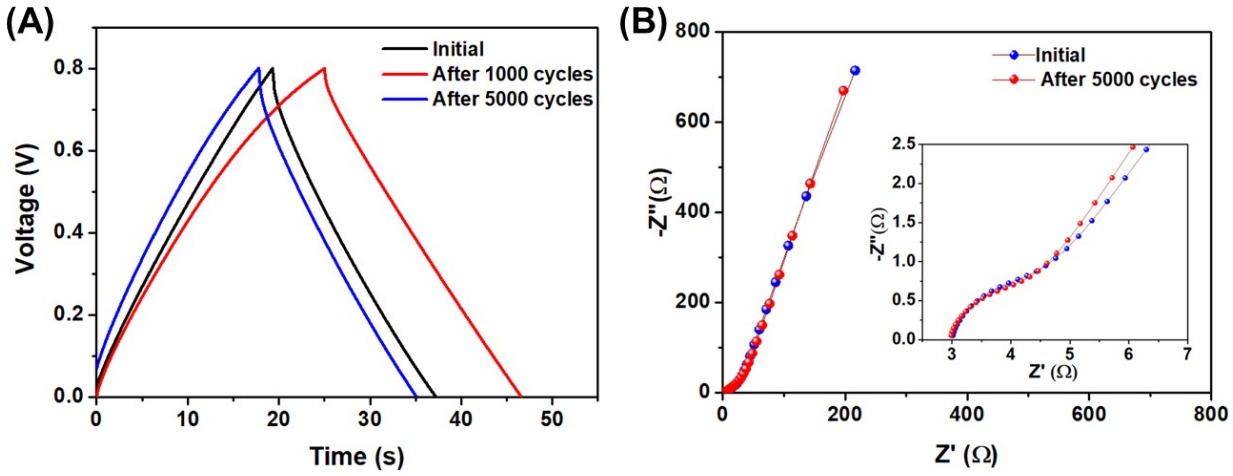

Figure. S7. (A) CD profiles of ReS_2 SSC and (B) Nyquist plot of ReS_2 SSC device during initial and after 5000 cycles of consecutive CD tests.

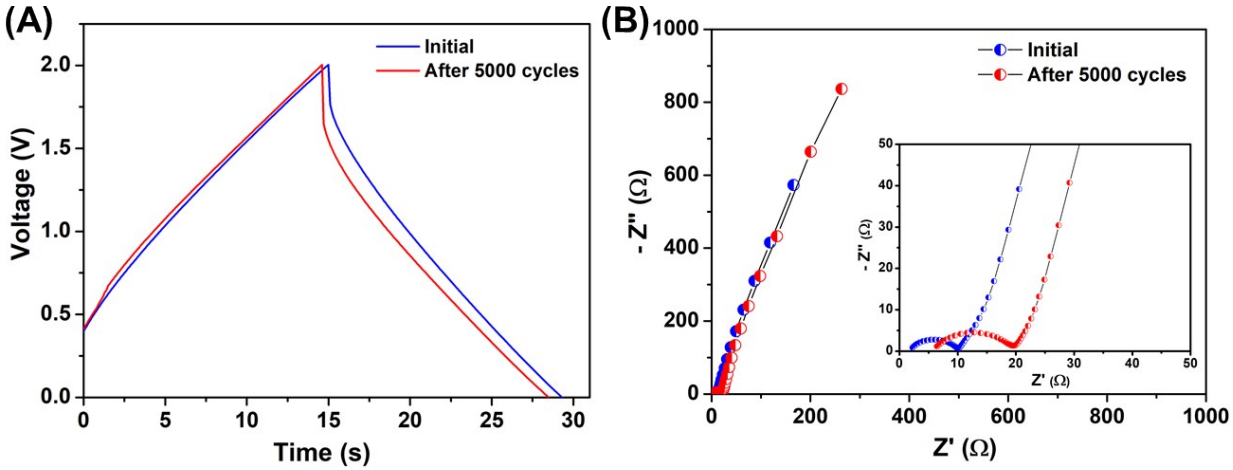

Figure. S8. (A) CD profiles of ReS_2 SSC and (B) Nyquist plot of ReS_2 SSC device during initial and after 5000 cycles of consecutive CD tests.

Table S1: Comparison on the performance of ReS_2 electrode with recently reported electrode materials.

S. No.	Materials	Electrolyte	Potential window (V)	Scan rate / Current density	Specific capacitance ($F\ g^{-1}$)	Ref
1	Few-layered MoS_2	LiOH	-0.7 to 0.0	5 mV s^{-1}	89	[5]
2	L-cysteine derived MoS_2	Na_2SO_4	-0.8 to 0.2	1 A g^{-1}	129	[8]
3	Ruthenium disulfide	H_2SO_4	0.0 to 0.8	0.5 mA cm^{-2}	85	[3]
4	Zinc sulfide	KOH	-0.2 to 0.2	5 mV s^{-1}	32	[9]
5	Samarium telluride	$LiClO_4$	-1.3 to 0.0	5 mV s^{-1}	144	[10]
6	$CuSbSe_2$	KOH	0.0 to 0.6	0.4 mA	34	[11]
7	Cu_3SbS_4	KOH	0.2 to 0.6	0.5 mA	20	[12]
8	accordion-like Ti_3C_2	Li_2SO_4	-0.9 to 0.3	2 mV s^{-1}	90	[13]
9	$Ti_3C_2T_x$	H_2SO_4	-0.6 to 0.1	1 A g^{-1}	116	[14]
10	Ruthenium oxide	H_2SO_4	0.0 to 1.2	20 mV s^{-1}	105	[15]
11	Porous Ruthenium oxide	H_2SO_4	-0.1 to 0.7	20 mV s^{-1}	50	[16]
12	Rhenium disulfide (ReS_2)	Li_2SO_4	-0.8 to 0.0	5 mV s^{-1}	162	This work
13	Rhenium disulfide (ReS_2)	Li_2SO_4	-0.8 to 0.0	0.5 mA cm^{-2}	189	This work

Table S2: Comparison on the performance of ReS_2 electrode with recently reported negative electrodes for supercapacitors.

S.NO	Electrode	Potential window (V)	Electrolyte	Scan rate / Current density	Specific capacitance (F g^{-1})	Ref.
1	Fe_2O_3 nanorod	-0.8 to 0.0	LiCl	5 mV s^{-1}	125	[17]
2	$CoFe_2O_4$	-1.2 to 0.0	KOH	2 m A	152	[18]
3	gC_3N_4-Fe_2O_3	-1 to 0.0	Li_2SO_4	1 A g^{-1}	167	[19]
4	FeP	-0.8 to 0.0	Na_2SO_4	1 mA cm^{-2}	149	[20]
5	MoO_2	-0.3 to +0.4	H_2SO_4	1 mA	140	[21]
6	MoO_2	-1.2 to -0.5	LiOH	5 mV s^{-1}	146	[22]
7	TiO_2	-1.4 to 0.0	Na_2SO_4	0.5 A g^{-1}	109	[23]
8	$FeWO_4$	-0.6 to 0.0	$LiNO_3$	10 mV s^{-1}	35	[24]
9	VN	-1.1 to -0.1	KOH	0.5 A g^{-1}	98	[25]
10	Fe_2N	-0.8 to 0.0	LiCl	10 mV s^{-1}	170	[26]
11	ReS_2	-0.8 to 0.0	Li_2SO_4	0.5 mA cm^{-2}	189	This work
12	ReS_2	-0.8 to 0.0	Li_2SO_4	5 mV s^{-1}	162	This work

Table S3: Comparison of specific capacitance, energy and power density of ReS_2 SSC device with reported SSC device

S.No.	SSC device	Specific capacitance (F g^{-1})	Energy density (Wh kg^{-1})	Power density (W kg^{-1})	Reference
1.	RuS_2	17	1.51	40	[3]
2.	FeS	4.62	2.56	726	[27]
3.	Ti_2CT_x	4.9	0.335	700	[28]
4.	2D MnO_2	248	1.9	297	[29]
5.	Ti_3C_2Tx	54	2	30	[30]
6.	Ni_2P	1.70	0.24	42	[31]
7.	Cu_3SbS_3	19	0.7	36	[12]
8.	Cu_3SbS_4	17.8	0.62	39	[12]
9.	Porous carbon	250	2.9	15	[32]
10.	ReS_2	35.75	3.17	1000	This work
11.	ReS_2	51.40	28.55	10,000	This work

Table S4: Comparison of energy density and power density of ReS_2 SSC device with reported TMO based supercapacitors device

S.No.	Device	Energy density (Wh kg^{-1})	Power density (W kg^{-1})	Reference
1.	AuNP/nano-Co_3O_4	25	400	[33]
2.	Graphene/MnO_2/CNT	8.9	106	[34]
3.	$ZnFe_2O_4$	4.47	277	[35]
4.	3D MnO_2/graphene	6.8	62	[36]
5.	$MnFe_2O_4$	10.25	3076	[37]
6.	N/NiO_x	20.3	240.9	[38]
7.	2D MnO_2	1.9	297	[39]
8.	$Co(OH)_2$	3.96	5000	[40]
9.	d-MnO_2	8.2	125	[41]
10.	ReS_2	3.17	1000	This work
11.	ReS_2	28.55	10,000	This work

References:

1 F. Qi, J. He, Y. Chen, B. Zheng, Q. Li, X. Wang, B. Yu, J. Lin, J. Zhou, P. Li, W. Zhang and Y. Li, Few-layered ReS2 nanosheets grown on carbon nanotubes: A highly efficient anode for high-performance lithium-ion batteries, *Chem. Eng. J.*, 2017, **315**, 10–17.

2 F. Qi, Y. Chen, B. Zheng, J. He, Q. Li, X. Wang, J. Lin, J. Zhou, B. Yu, P. Li and W. Zhang, Hierarchical architecture of ReS 2 /rGO composites with enhanced electrochemical properties for lithium-ion batteries, *Appl. Surf. Sci.*, 2017, **413**, 123–128.

3 K. Krishnamoorthy, P. Pazhamalai and S. J. Kim, Ruthenium sulfide nanoparticles as a new pseudocapacitive material for supercapacitor, *Electrochim. Acta*, 2017, **227**, 85–94.

4 P. Pazhamalai, K. Krishnamoorthy, M. S. P. Sudhakaran and S. J. Kim, Fabrication of High-Performance Aqueous Li-Ion Hybrid Capacitor with LiMn2O4 and Graphene, *ChemElectroChem*, 2017, **4**, 396–403.

5 K. Krishnamoorthy, P. Pazhamalai, G. K. Veerasubramani and S. J. Kim, Mechanically delaminated few layered MoS2 nanosheets based high performance wire type solid-state symmetric supercapacitors, *J. Power Sources*, 2016, **321**, 112–119.

6 G. K. Veerasubramani, M. S. P. Sudhakaran, N. R. Alluri, K. Krishnamoorthy, Y. S. Mok and S. J. Kim, Effective use of an idle carbon-deposited catalyst for energy storage applications, *J. Mater. Chem. A*, 2016, **4**, 12571–12582.

7 K. Krishnamoorthy, P. Pazhamalai, S. Sahoo and S. J. Kim, Titanium carbide sheet based high performance wire type solid state supercapacitors, *J. Mater. Chem. A*, 2017, **5**, 5726–5736.

8 K. J. Huang, J. Z. Zhang, G. W. Shi and Y. M. Liu, Hydrothermal synthesis of molybdenum disulfide nanosheets as supercapacitors electrode material, *Electrochim.*

Acta, 2014, **132**, 397–403.

9 R. Ramachandran, M. Saranya, P. Kollu, B. P. C. Raghupathy, S. K. Jeong and A. N. Grace, Solvothermal synthesis of Zinc sulfide decorated Graphene (ZnS/G) nanocomposites for novel Supercapacitor electrodes, *Electrochim. Acta*, 2015, **178**, 647–657.

10 V. S. Kumbhar, A. C. Lokhande, N. S. Gaikwad and C. D. Lokhande, Synthesis of samarium telluride thin films by successive ionic layer adsorption and reaction (SILAR) method for supercapacitor application, *Mater. Sci. Semicond. Process.*, 2016, **46**, 29–34.

11 K. Ramasamy, R. K. Gupta, S. Palchoudhury, S. Ivanov and A. Gupta, Layer-structured copper antimony chalcogenides (CuSbSexS2-x): Stable electrode materials for supercapacitors, *Chem. Mater.*, 2015, **27**, 379–386.

12 K. Ramasamy, R. K. Gupta, H. Sims, S. Palchoudhury, S. Ivanov and A. Gupta, Layered ternary sulfide CuSbS2 nanoplates for flexible solid-state supercapacitors, *J. Mater. Chem. A*, 2015, **3**, 13263–13274.

13 Y. Tian, C. Yang, W. Que, Y. He, X. Liu, Y. Luo, X. Yin and L. B. Kong, Ni foam supported quasi-core-shell structure of ultrathin Ti3C2 nanosheets through electrostatic layer-by-layer self-assembly as high rate-performance electrodes of supercapacitors, *J. Power Sources*, 2017, **369**, 78–86.

14 T. Zhao, J. Zhang, Z. Du, Y. Liu, G. Zhou and J. Wang, Dopamine-derived N-doped carbon decorated titanium carbide composite for enhanced supercapacitive performance, *Electrochim. Acta*, 2017, **254**, 308–319.

15 C. C. Hu, Y. H. Huang and K. H. Chang, Annealing effects on the physicochemical characteristics of hydrous ruthenium and ruthenium-iridium oxides for electrochemical

supercapacitors, *J. Power Sources*, 2002, **108**, 117–127.

16 V. D. Patake and C. D. Lokhande, Chemical synthesis of nano-porous ruthenium oxide (RuO 2) thin films for supercapacitor application, *Appl. Surf. Sci.*, 2008, **254**, 2820–2824.

17 Y. Li, Q. Li, L. Cao, X. Cui, Y. Yang, P. Xiao and Y. Zhang, The impact of morphologies and electrolyte solutions on the supercapacitive behavior for Fe2O3 and the charge storage mechanism, *Electrochim. Acta*, 2015, **178**, 171–178.

18 K. V. Sankar, S. Shanmugapriya, S. Surendran, S. C. Jun and R. K. Selvan, Facile hydrothermal synthesis of carbon-coated cobalt ferrite spherical nanoparticles as a potential negative electrode for flexible supercapattery, *J. Colloid Interface Sci.*, 2018, **513**, 480–488.

19 L. Xu, J. Xia, H. Xu, S. Yin, K. Wang, L. Huang, L. Wang and H. Li, Reactable ionic liquid assisted solvothermal synthesis of graphite-like C3N4 hybridized α-Fe2O3 hollow microspheres with enhanced supercapacitive performance, *J. Power Sources*, 2014, **245**, 866–874.

20 J. Luo, Z. Zheng, A. Kumamoto, W. I. Unah, S. Yan, Y. H. Ikuhara, X. Xiang, X. Zu and W. Zhou, PEDOT coated iron phosphide nanorod arrays as high-performance supercapacitor negative electrodes, *Chem. Commun.*, 2018, **54**, 794–797.

21 J. Rajeswari, P. S. Kishore, B. Viswanathan and T. K. Varadarajan, One-dimensional MoO2 nanorods for supercapacitor applications, *Electrochem. commun.*, 2009, **11**, 572–575.

22 X. Li, J. Shao, J. Li, L. Zhang, Q. Qu and H. Zheng, Ordered mesoporous MoO2 as a high-performance anode material for aqueous supercapacitors, *J. Power Sources*, 2013, **237**, 80–83.

23 W. Guo, Y. Li, Y. Tang, S. Chen, Z. Liu, L. Wang, Y. Zhao and F. Gao, TiO2 Nanowire Arrays on Titanium Substrate as a Novel Binder-free Negative Electrode for Asymmetric Supercapacitor, *Electrochim. Acta*, 2017, **229**, 197–207.

24 N. Goubard-Bretesché, O. Crosnier, C. Payen, F. Favier and T. Brousse, Nanocrystalline FeWO4 as a pseudocapacitive electrode material for high volumetric energy density supercapacitors operated in an aqueous electrolyte, *Electrochem. commun.*, 2015, **57**, 61–64.

25 R. Wang, X. Yan, J. Lang, Z. Zheng and P. Zhang, A hybrid supercapacitor based on flower-like Co(OH)2 and urchin-like VN electrode materials, *J. Mater. Chem. A*, 2014, **2**, 12724–12732.

26 C. Zhu, P. Yang, D. Chao, X. Wang, X. Zhang, S. Chen, B. K. Tay, H. Huang, H. Zhang, W. Mai and H. J. Fan, All Metal Nitrides Solid-State Asymmetric Supercapacitors, *Adv. Mater.*, 2015, **27**, 4566–4571.

27 S. S. Karade, P. Dwivedi, S. Majumder, B. Pandit and B. R. Sankapal, First report on a FeS-based 2 V operating flexible solid-state symmetric supercapacitor device, *Sustain. Energy Fuels*, 2017, **1**, 1366–1375.

28 R. B. Rakhi, B. Ahmed, M. N. Hedhili, D. H. Anjum and H. N. Alshareef, Effect of Postetch Annealing Gas Composition on the Structural and Electrochemical Properties of Ti2CTx MXene Electrodes for Supercapacitor Applications, *Chem. Mater.*, 2015, **27**, 5314–5323.

29 R. S. Kalubarme, H. S. Jadhav and C. J. Park, Electrochemical characteristics of two-dimensional nano-structured MnO 2 for symmetric supercapacitor, *Electrochim. Acta*, 2013, **87**, 457–465.

30 A. M. Navarro-Suárez, K. L. Van Aken, T. Mathis, T. Makaryan, J. Yan, J. Carretero-González, T. Rojo and Y. Gogotsi, Development of asymmetric supercapacitors with titanium carbide-reduced graphene oxide couples as electrodes, *Electrochim. Acta*, 2018, **259**, 752–761.

31 W. Du, R. Kang, P. Geng, X. Xiong, D. Li, Q. Tian and H. Pang, New asymmetric and symmetric supercapacitor cells based on nickel phosphide nanoparticles, *Mater. Chem. Phys.*, 2015, **165**, 207–214.

32 D. W. Wang, F. Li, M. Liu, G. Q. Lu and H. M. Cheng, 3D aperiodic hierarchical porous graphitic carbon material for high-rate electrochemical capacitive energy storage, *Angew. Chemie - Int. Ed.*, 2008, **47**, 373–376.

33 Y. Tan, Y. Liu, L. Kong, L. Kang and F. Ran, Supercapacitor electrode of nano-Co3O4 decorated with gold nanoparticles via in-situ reduction method, *J. Power Sources*, 2017, **363**, 1–8.

34 Y. Cheng, S. Lu, H. Zhang, C. V. Varanasi and J. Liu, Synergistic Effects from Graphene and Carbon Nanotubes Enable Flexible and Robust Electrodes for High-Performance Supercapacitors, *Nano Lett.*, 2012, **12**, 4206–4211.

35 S. S. Raut and B. R. Sankapal, First report on synthesis of ZnFe2O4 thin film using successive ionic layer adsorption and reaction: Approach towards solid-state symmetric supercapacitor device, *Electrochim. Acta*, 2016, **198**, 203–211.

36 Y. He, W. Chen, X. Li, Z. Zhang, J. Fu, C. Zhao and E. Xie, Freestanding Three-Dimensional Graphene/MnO 2 Composite Networks As Ultralight and Flexible Supercapacitor Electrodes, *ACS Nano*, 2013, **7**, 174–182.

37 K. V. Sankar and R. K. Selvan, The preparation of MnFe2O4 decorated flexible graphene

wrapped with PANI and its electrochemical performances for hybrid supercapacitors, *RSC Adv.*, 2014, **4**, 17555–17566.

38 K. Chen, J. Liu, H. Bian, J. Wei, W. Wang and Z. Shao, Ingenious preparation of N/NiO x co-doped hierarchical porous carbon nanosheets derived from chitosan nanofibers for high-performance supercapacitors, *Nanotechnology*, 2020, **31**, 335713.

39 R. S. Kalubarme, H. S. Jadhav and C.-J. Park, Electrochemical characteristics of two-dimensional nano-structured MnO2 for symmetric supercapacitor, *Electrochim. Acta*, 2013, **87**, 457–465.

40 A. D. Jagadale, V. S. Kumbhar, D. S. Dhawale and C. D. Lokhande, Performance evaluation of symmetric supercapacitor based on cobalt hydroxide [Co(OH)2] thin film electrodes, *Electrochim. Acta*, 2013, **98**, 32–38.

41 W. Xiao, W. Zhou, H. Yu, Y. Pu, Y. Zhang and C. Hu, Template synthesis of hierarchical mesoporous δ-MnO 2 hollow microspheres as electrode material for high-performance symmetric supercapacitor, *Electrochim. Acta*, 2018, **264**, 1–11.